Journal of Hazardous Materials 443 (2023) 130311

Contents lists available at ScienceDirect

Journal of Hazardous Materials

journal homepage: www.elsevier.com/locate/jhazmat

Research Paper

Wildland-urban interface fire ashes as a major source of incidental nanomaterials

Talal Alshehri [a,b], Jingjing Wang [a], Sheryl A. Singerling [c], Julien Gigault [d], Jackson P. Webster [e], Sandrine J. Matiasek [f], Charles N. Alpers [g], Mohammed Baalousha [a,*]

[a] Center for Environmental Nanoscience and Risk, Department of Environmental Health Sciences, Arnold School of Public Health, University of South Carolina, Columbia, SC 29201, United States
[b] Environmental Health Department, College of Public Health, Imam Abdulrahman Bin Faisal University, Dammam 31441, Saudi Arabia
[c] National Center for Earth and Environmental Nanotechnology Infrastructure (NanoEarth, Institute for Critical Technology and Applied Science, Virginia Polytechnic Institute and State University, Blacksburg, VA 24061, United States
[d] TAKUVIK, Université Laval/CNRS, IRL 3376, G1V 0A6 Québec, Canada
[e] Department of Civil Engineering, California State University Chico, 400 W 1st St, Chico, CA 95929, United States
[f] Department of Earth and Environmental Sciences, California State University Chico, 400 W 1st St, Chico, CA 95929, United States
[g] US Geological Survey, California Water Science Center, 6000 J Street, Sacramento, CA 95819, United States

HIGHLIGHTS

- Metal and metalloid concentrations in WUI fire ash were determined.
- The composition and size of incidental nanomaterial in WUI fire ash were determined.
- Fire ash contain high metal and metalloid concentrations in the form of incidental nanomaterials.
- Ti, Cu, Fe, Zn, Mn, Pb, and Cr-bearing INMs were detected in WUI fire ash.
- Incidental nanomaterial sizes varied from < 50 nm to a few hundred nms.

GRAPHICAL ABSTRACT

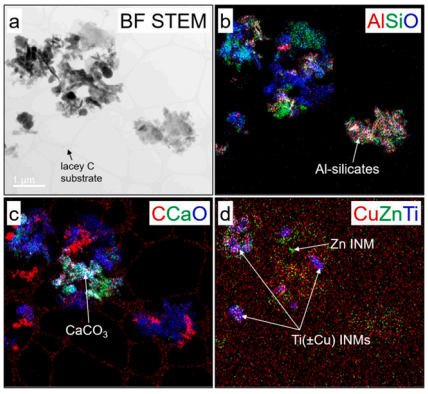

ARTICLE INFO

Editor: Dr. T Meiping

Keywords:
Incidental nanomaterials
Wildland-urban interface fire
Fire ash
Metals and metalloids

ABSTRACT

Although metal and metalloid concentrations in wildfire ashes have been documented, the nature and concentrations of incidental nanomaterials (INMs) in wildland-urban interface (WUI) fire ashes have received considerably less attention. In this study, the total metal and metalloid concentrations of 57 vegetation, structural, and vehicle ashes and underlying soils collected at the WUI following the 2020 fire season in northern California — North Complex Fire and LNU Lightning Complex Fire — were determined using inductively coupled plasma-time of flight-mass spectrometry after microwave-assisted acid digestion. The concentrations of Ti, Zn, Cu, Ni, Pb, Sn, Sb, Co, Bi, Cr, Ba, As, Rb, and W are generally higher in structural/vehicle-derived ashes than in vegetation-derived ashes and soils. The concentrations of Ca, Sr, Rb, and Ag increased with increased combustion

* Corresponding author.
E-mail address: mbaalous@mailbox.sc.edu (M. Baalousha).

https://doi.org/10.1016/j.jhazmat.2022.130311
Received 29 July 2022; Received in revised form 18 October 2022; Accepted 31 October 2022
Available online 2 November 2022

completeness (*e.g.,* black ash < gray ash < white ash), whereas those of C, N, Zn, Pb, and In decreased with increased combustion completeness. The concentration of anthropogenic Ti — determined by mass balance calculations and shifts in Ti/Nb above the natural background ratios — was highest in vehicle ash (median: 30.8 g kg^{-1}, range: 4.5–41.0 g kg^{-1}) followed by structural ash (median: 5.5 g kg^{-1}, range: of 0–77.4 g kg^{-1}). Various types of carbonaceous INM (*e.g.,* amorphous carbon, turbostratic-like carbon, and carbon associated with zinc oxides) and metal-bearing INMs (*e.g.,* Ti, Cu, Fe, Zn, Mn, Pb, and Cr) with sizes between few nanometers to few hundreds of nanometers were evidenced in ashes using transmission electron microscopy, including energy dispersive X-ray spectroscopy. Overall, this study demonstrates the abundance of a variety of metals and metalloids in the form of INMs in WUI fire ashes. This study also highlights the need for further research into the formation, transformation, reactivity, fate, and effects of INMs during and following fires at the WUI.

1. Introduction

Fire (*i.e.,* wildfire, land-management burning, and agricultural burning) is a frequent global phenomenon affecting 3–5 million km^2 annually around the world, burning ~ 4 % of the Earth's vegetated land (Van Der Werf et al., 2017). Wildfires are also a frequent phenomenon across the United States, with those in the eastern states (*e.g.,* including and east of Minnesota, Iowa, Missouri, Arkansas, and Louisiana) occurring more frequently but typically being smaller in scale than those in western states (U.S. Environmental Protection Agency, 2016). For instance, in 2020, more than 33,000 fires burned approximately 700,000 acres in the eastern states, whereas almost 26,000 wildfires burned 9.5 million acres in the western states (U.S. Environmental Protection Agency, 2016). Wildfires have become increasingly destructive in recent years in the western United States, particularly in California, due to rising temperatures from climate change, a preponderance of fuels due to long-term fire suppression, and an increased population living in proximity to wildland vegetation, *i.e.,* at the wildland-urban interface (Miller et al., 2009). The area burned by wildfires across the United States has increased from 1.3 million acres in 1983–7.1 million acres in 2021, with the 2020 fire season consuming a record 10.1 million acres of wildland and destroying approximately 18,000 structures, including 9600 homes (Hoover and Hanson, 2021). Currently, wildfires are a contentious issue due to increases in fire frequency, size, severity, and the spread of fires into the built environment, resulting in increased emissions of contaminants of emerging concern (Bladon et al., 2014; Brito et al., 2017). These contaminants threaten ecosystems with implications for air and water pollution and related problems for environmental and human health (Bladon et al., 2014; Brito et al., 2017). Fire activity at the wildland-urban interface (WUI) and the associated environmental and human health impacts are projected to increase globally due to climate and societal changes, making an understanding of the impacts of wildfires more crucial than ever (Scholze et al., 2006).

Ash is the particulate residue that remains *in situ* after fire (Bodí et al., 2014). Ash produced by wildfires is a heterogeneous material composed mainly of charred organic materials, oxides and hydroxides of base cations (*e.g.,* Ca^{2+}, Mg^{2+}, and K^{+}), and a mixture of organic and inorganic contaminants. Fire releases a complex mix of particles, liquids, and gaseous compounds, which depend on the type and efficiency of combustion. Pollutants released by fires, and concentrated in the ashes, include pyrogenic carbon, polycyclic aromatic hydrocarbons (PAHs), polychlorinated dioxins and furans (PCDD/FE), volatile organic compounds (VOCs), metals, metalloids, incidental nanomaterials (INMs, particles in the size range of 1–100 nm unintentionally formed as a result of direct or indirect human influence), environmentally persistent free radicals (EPFRs), nutrients, and other contaminants (Bodí et al., 2014). These fire-emitted contaminants are known to affect the health of millions of people and other living organisms in the surrounding environment (Oliveira-Filho et al., 2018).

Combustion processes enrich ash in trace metals and metalloids such as As, Cr, Cu, Pb, Hg, Ni, and Zn (Burton et al., 2016; Wan et al., 2021). For instance, several studies reported elevated metal concentrations in forest-fire ash (*e.g.,* 67–598 mg Mn kg^{-1}, 51–122 mg Pb kg^{-1}) and in post-fire soil (*e.g.,* 471–1429 mg Mn kg^{-1}) (Campos et al., 2016; Parra et al., 1996), likely in the form of INMs. Additional pollutants might be emitted at the WUI due to the combustion of construction materials (*e.g.,* wood, roofing, vinyl, plumbing, electrical, paints), household items (*e.g.,* furniture, cooking utensils, ceramics, rubber, plastics), industrial solvents, petroleum products, automotive components, tires, and consumer electronics (Radeloff et al., 2018). For instance, ash from buildings burned in WUI fires can have substantially elevated levels of diverse trace elements such as Pb, Cr, As, Cu, and Zn (Plumlee et al., 2013). Many construction materials and consumer products use metal and engineered particles (*e.g.,* pigments and nanoparticles). However, there is currently limited knowledge of the occurrence, concentrations, and properties of INMs forming from WUI fires. For instance, multiwall carbon nanotubes were detected in wildfire emissions (Lara-Romero et al., 2017). Inorganic INMs could form *via* precipitation, condensation, oxidation, and reduction of inorganic material in fire fuel (Griffin et al., 2018). To date, there is limited information on the concentrations of metals and the nature and concentrations of INMs in fire ash generated from fire in the built environment.

Furthermore, the concentrations of pyrogenic carbon and inorganic contaminants in ashes depend on the fire conditions. Low combustion completeness (*e.g.,* T < 450 °C) forms black ash with organic carbon as the main component. At high combustion completeness (*e.g.,* T > 450 °C), most organic carbon is volatilized, leaving behind mineral ash (or white ash) with Ca, Mg, Na, K, and Si in the form of inorganic carbonates (Bodí et al., 2014). At a higher combustion temperature (T > 850 °C), the most common inorganics remaining are oxides (Bodí et al., 2014). The concentrations of metals and metalloids in ashes also vary depending on fire severity as combustion processes release metals stored in plants (Kaschl et al., 2002; Sipos et al., 2005), soil organic matter (Obrist, 2007; Rutter et al., 2011), and structural materials by either volatilization into the atmosphere (*e.g.,* Hg) or accumulation on the soil surface within the ash.

The overarching aim of this study is to determine the concentrations of metals, metalloids, and INMs in WUI fire ash from different fuel sources and combustion completeness and to characterize the properties of INMs that form as a result of fires at the WUI. To do this, we use ashes collected after the 2020 fire season in the western United States, including those collected from the North Complex Fire and LNU Lightning Complex Fire in northern California.

2. Materials and methods

2.1. Study sites

Two WUI fires that burned during the 2020 California fire season were investigated in this study, including the North Complex (NC) Fire and the LNU Lightning Complex Fire (Fig. S1).

The North Complex Fire (NC) is the seventh largest in California history (as of June 2022) and the second largest recorded in the northern Sierra Nevada. It burned 1290 km^2 and destroyed 2455 structures in the Feather River watershed, primarily within the Plumas National Forest, between August 17 and December 3, 2020. The distribution of burn severity within the fire perimeter was 2% low, 8% moderate, and 89% high (Fig. S1a) (inciweb, 2022). The land use within the burned area was

84% evergreen forest and 12% shrub/scrub; the elevation averaged 1153 m and ranged from 260 to 2132 m (Fig. S2).

Fire ash and soil samples were collected in the Berry Creek Census Designated Place, where most structures were destroyed (**SI** Table S1 **and** Fig. S2). Within Berry Creek, we sampled a neighborhood surrounding Madrone Lake with a high density of burned structures. The general setting is indicative of the western slope of the Sierra Nevada in California in the 300–750 m elevation range in terms of geology and vegetation. The area is characterized by steep terrain underlain by granitic and metavolcanic bedrock. The soils vary based on the underlying parent formations, with decomposed granite soils in some areas and the metavolcanic rocks forming "red dirt" soils, including the Hartsmill Series (detailed soil series description is provided in the SI). At lower elevations (about 300 m), vegetation is characterized by manzanita (*Arctostaphylos spp.*), toyon (*Heteromeles arbutifolia*), interior live oak (*Quercus wislizeni*), California black oak (*Quercus kelloggii*), Pacific poison oak (*Toxicodendron diversilobum*), and very scattered ponderosa pine (*Pinus ponderosa*). At higher elevations (about 750 m), vegetation cover is characterized by California mixed conifer, including black oak (*Quercus velutina*), California live oak (*Quercus agrifolia*), Pacific madrone (*Arbutus menziesii*), ponderosa pine (*Pinus ponderosa*), Douglas-fir (*Pseudotsuga menziesii*), and mixed shrub species.

The LNU Lightning Complex Fire is the sixth largest in California history (as of June 2022). It burned 1470 km^2 and destroyed 1491 structures in Colusa, Lake, Napa, Sonoma, Solano, and Yolo Counties, approximately 60 km west of Sacramento, between August 17 and October 2, 2020 (CALFire, 2022). The distribution of burn severity within the fire perimeter was 12 % low, 39 % moderate, and 49 % high (Fig. S1b). Land use within the fire perimeter comprised of 57 % shrub/scrub, 19 % herbaceous, 12 % evergreen forest, and 1.4 % developed (Fig. S3). Elevation within the fire footprint was on average 370 m and ranged between 35 and 924 m.

Fire ash samples were collected from vegetated areas and the built environment in Napa and Solano counties near Lake Berryessa (SI Table S1 and Fig. S3). The general setting is typical of the Coast Ranges in central California. Elevation of valleys in the Lake Berryessa region generally range from 90 to 120 m, with ridge elevations from 600 to 900 m. The geology of the Lake Berryessa region has a diversity of rock types, including deformed, metamorphosed sedimentary and volcanic rocks of the Franciscan Complex; sedimentary and volcanic rocks of the Great Valley Group; igneous rocks of the Clear Lake Volcanics, and alluvium (Moores et al., 2020). Soils in the area are typically well-drained and include the Henneke Series, formed from weathered, ultramafic rocks such as serpentinite; the Forward Series, formed from weathered volcanic rocks; and the Bressa Series, formed from weathering of sandstone and shale. Vegetation is diverse in the Lake Berryessa region and varies by elevation. Valley floors typically have grasslands and valley oak woodlands with riparian habitats along creeks and streams; at mid-elevations, hardwood forests have various oak species, gray pine (*Pinus sabiniana*), Pacific madrone, and various chaparral plant species; higher elevations support Douglas-fir, ponderosa pine, incense cedar (*Calocedrus decurrens*), and various montane chaparral plant species (Moores et al., 2020).

2.2. Sample collection

A total of 62 ash, underlying soil, and unburned vegetation samples were collected during October to November 2020 in the two fire-affected areas (Table S1). In the North Complex Fire area, the collected samples include four ash samples from burned structures, five ash samples from burned vehicles, six ash samples from burned vegetation, and eight underlying soil samples. In the LNU Lightning Complex Fire area, the collected samples include 25 ash samples from burned structures, four ash samples from burned vehicles, four ash samples from burned vegetation, and five samples of unburned vegetation. In addition, a sample of air-fall ash was collected from a car's windshield during the 2019 fire season near the North Complex Fire area; care was taken to avoid contact with the glass to avoid previously deposited dust or debris. All samples were collected prior to any rain or other precipitation. The ash samples were collected from various sources, including residential structures, garages, vehicles, vegetation, and soils representing low to high burn severity (Table S1). The burned structures included residences, a convenience store, and storage sheds; burned vehicles included automobiles, tractors, and a boat on a trailer. Vegetation types sampled included various oak and pine species, manzanita (*Arctostaphylos spp.*), chamise, (*Adenostoma fasciculatum*) and grasses.

Within the NC Fire area, ash and soil samples were collected from the neighborhood surrounding Madrone Lake (Fig. S2 **and** Table S1). Undisturbed ash was carefully scraped from the soil surface with a disposable plastic scoop and collected to represent average (mixed) sources. In burned structures from the NC Fire area, ash was collected from multiple locations within the structure's footprint and combined to form a representative composite sample. Sampling burned structures is difficult because the ash is not uniform like vegetation ash. It is often a mixture of wallboard, insulation, and large debris, all mixed with the combusted material residuals. To collect underlying soil, the area where surface ash was collected was carefully cleared of ash, and the underlying soil was collected using a plastic scoop from two soil depths (0–2 cm, NC 1 C, NC 6 A, NC 10B, NC 12B, and NC 13B; 10–15 cm, NC 6B, NC 12 C, and NC 13 C). Detailed soil series descriptions are provided in the SI section. All samples were collected in acid-washed high-density polyethylene (HDPE) wide-mouth bottles and labeled.

Within the LNU Lightning Complex Fire area, undisturbed ash samples were carefully collected from burned structures and vegetation to represent specific location sources; ash samples were collected from multiple locations (*e.g.,* kitchen, living room, bedroom, garage, foundation, *etc.*) within each residential structure; detached structures adjacent to residences (*e.g.,* sheds, barns, and trailers) and a commercial structure (convenience store) were also sampled (Fig. S3 and Table S1). Ash samples were collected with disposable plastic scoops and placed into zippered plastic bags.

2.3. Preparation of ashes and unburned vegetation

All ashes were homogenized using a mortar and a pestle. Unburned vegetation samples were washed thrice with ultra-high-purity water to rinse off dust particles and then dried in an oven at 50 °C to remove moisture without disturbing nanomaterials in the samples (Peacock, 1992). The dried vegetation samples were then homogenized using a mortar and a pestle. The homogenized ashes and unburned vegetation were sieved using a 10-mesh (2 mm pore size) nylon sieve (Zhangxing Instrument, Hangzhou, Zhejiang, China) to remove large particles. The sieved samples were stored in 250 ml acid-washed HDPE bottles in a −20 °C freezer before further treatment.

2.4. Carbon and nitrogen analysis

Carbon and nitrogen analysis was performed using an ECS 4010 Elemental Analyzer/ZeroBlank Autosampler (Costech Analytical Technologies). Samples were loaded into tin capsules and combusted (localized temperature up to 1800 °C) to determine carbon and nitrogen isotopic ratios simultaneously. Two laboratory standards, USGS40 and USGS41, were analyzed for every 12 unknown samples in each analytical sequence, allowing instrument drift to be corrected if required.

2.5. Digestion and metal analysis

One hundred mg of each sample was weighed into a polytetrafluoroethylene (PTFE) digestion vessel. Digestion reagents were added in the following order: 9 ml of distilled HNO_3, 3 ml of distilled HF, and 2 ml of H_2O_2. The acid digestion was performed in a Multiwave microwave (Multiwave Pro, Anton Paar, Graz, Austria) at a constant power of

1500 W for 60 min, preceded by a 15-minute ramping time to reach the desired power. The digestate was then evaporated in two steps using the same microwave system to remove non-reacted HF. The first evaporation was performed with 10 min of ramping time followed by 9 min of holding time at 1500 W. Then, 3 ml of distilled HNO_3 was added into the vessel to dissolve any insoluble fluoride salts. The second evaporation was performed with 10 min of ramping time followed by 3 min of holding time at 1500 W. The digested samples were then diluted in 10% HNO_3 (trace metal grade, Fisher Chemical, Fair Lawn, NJ, USA) and stored until total metal analysis.

Total metal concentrations were determined using an inductively coupled plasma-time of flight-mass spectrometer (ICP-TOF-MS, TOFWERK, Switzerland). Mass spectra calibration and routine tuning were performed prior to analysis every day to achieve maximum sensitivity. Elemental concentration calibration was established using a series of ionic standards prepared in 1% HNO_3 from commercially available ICP multi-element standards (BDH Chemicals, Radnor, PA, USA). Internal standards (ICP Internal Element Group Calibration Standard, BDH Chemicals, Radnor, PA, USA) were applied to monitor signal drift for quality control. The instrument operating conditions are presented in Table S2**,** and the monitored isotopes are listed in Table S3. Dissolved multi-element standards were prepared in 1 % HNO_3 from commercially available ICP standards (BDH Chemicals, Radnor, PA, USA), with concentrations ranging from 0.001 to 100 μg L^{-1}. Internal standards (ICP Internal Element Group Calibration Standard, BDH Chemicals, Radnor, PA, USA) were monitored simultaneously for quality control. All isotopes were analyzed in collision mode with a helium and hydrogen gas mixture.

The recovery of the digestion procedure was determined by digesting and analyzing two standard reference materials for trace elements in coal fly ash: NIST SRM 1663 C (NIST, Gaithersburg, MD, USA) and BCR-176R (IRMM, Retieseweg, Geel, Belgium). For 1663 C, the recovery varied between 82 % and 125 % for most elements (Table S3). Cu exhibited high recovery of 137 % and U exhibited a low recovery of 67 %. For BCR-176R, the recovery varied between 77 % and 105 % for most elements. Barium and Th exhibited low recoveries of 42 % and 70 %, respectively, while Zn and Se exhibited high recoveries of 131 % and 146 %, respectively (Table S3). All elements' relative standard deviation was < 15 %, indicating good precision.

2.6. Transmission electron microscopy

A select set of samples was further characterized by transmission electron microscopy (TEM) to identify the various types of INMs present in the fire ashes. These samples were selected to represent different endmembers based on their elemental compositions. TEM was used to study the morphology, dimensions, crystallinity, and elemental compositions of the INMs in eight ash samples: A13, A31, A81, A122, A124, A131, A132, and AD. The samples were prepared for TEM analyses by the drop-casting method using suspensions of WUI fire ash dispersed in methanol. The suspensions were shaken, let to sit for several minutes, and then dropped onto LC300-Cu-150 TEM grids (Electron Microscopy Sciences), which consist of a lacey carbon support layer attached to a 300-mesh copper grid. The TEM samples were stored in a vacuum desiccator for at least 24 h before being analyzed. TEM data were collected at the Nanoscale Characterization and Fabrication Laboratory at Virginia Polytechnic Institute and State University on a JEOL JEM 2100 S/TEM, operated at 200 kV. TEM bright field images were acquired with a Gatan Ultrascan 1000XP CCD camera. Energy dispersive x-ray spectroscopy (EDS) elemental maps were obtained using a JEOL genuine 60 mm^2 Silicon Drift Detector.

3. Results and discussion

3.1. Ash source and color

Ashes were grouped into four categories based on their source, including 10 vegetation, 29 structural, nine vehicle, and an atmospheric-deposition ash. In addition to the ashes, five unburned vegetation and eight soil samples were digested and analyzed for total metal concentration. Ashes were also grouped into five categories based on their color as observed by the naked eye and included 13 black, 11 gray, 18 white, eight gray/brown, and seven red/brown ashes (Fig. S4). Ash color is a qualitative parameter that can be used to describe the completeness of combustion and thus fire temperature (Dūdaitė et al., 2011). Depending on the consumption of organic matter, ash color ranges from black indicating charring to white indicating complete ashing (Bodí et al., 2011). For instance, combustion of pine needles and leaf litter at 350 °C generated black ash, whereas combustion of pine needles at 550 °C and leaf litter at 450 °C generated white ash (Dūdaitė et al., 2011). Wood ash generated at 250 °C is brown because of the onset of pyrolysis and shrinkage at that temperature and turns black above 300 °C (Ragland et al., 1991). Moderate-intensity fire (300–400 °C) produces black ash because the vegetation is not destroyed, but high-intensity fire (> 500 °C) produces light gray or white ash (Iglesias et al., 1997) composed mainly of alkaline (Ca, K, Mg) oxides (Goforth et al., 2005). The ash color is also impacted by the amount of Fe, which can vary from orange to deep red, brown, or white to yellow (Ahmaruzzaman, 2010). For instance, one structural ash (A92) was red due to its high Fe content (32 % of ash weight, hereafter wt%). All other red/brown samples were soil samples. Below we discuss the elemental compositional trends of all ash samples based on their sources and colors.

3.2. Elemental concentrations in ash from distinct source

The elemental composition of WUI fire ashes can vary depending on the fuel type. Fig. 1 presents the elemental concentrations in ashes, which are ordered based on the increase/decrease in their concentration among the different ash sources. For all ashes, C concentrations ranged from 0.6 to 47.6 wt% and increase in the following order: soil < structure < vegetation < vehicle (Fig. 1a). The total major and trace metal (Ca + metals + metalloids) concentrations range from 2.4 to 47.0 wt% and increase in the following order: soil < burned vegetation < structure < vehicles (Fig. 1b). The total major and trace metal concentrations in the different ash types vary as follows: underlying soils range from 2 to 12.8 wt% with a mean of 5.8 ± 3.7 wt%, vegetation ashes vary from 3.8 to 11.5 wt% with a mean of 8.5 ± 2.5 wt%, structural ashes vary from 5.8 to 47 wt% with a mean of 12.6 ± 7.7 wt%, and vehicle ashes vary from 6.7 to 22.7 wt% with a mean of 14.7 ± 4.5 wt% (Fig. 1b).

Overall, Ti, Zn, Cu, Ni, Pb, Sb, Sn, Co, Bi, and Cr contents increase in the following order: unburned vegetation < vegetation ash < ~ soil < structure < vehicle (Fig. 1**c-l**). Nitrogen concentration is highest in vehicle ashes (*e.g.,* median: 0.31, range: 0–0.47 wt%) followed by vegetation (*e.g.,* median: 0.19, range: 0–0.55 wt%)), soil (*e.g.,* median: 0.09, range: 0.07–0.16 wt%), and structural ashes (*e.g.,* median: 0.05, range: 0–0.52 wt%) (Fig. 1m). Barium, Ca, As, Rb, and W have the highest concentrations in structural ashes and lowest concentrations in soils (Fig. 1n-r). Sr and Mn are at their highest concentrations in vegetation ashes (Fig. 1s-t). These trends are consistent with the natural occurrence of these metals in vegetation and the uses of these metals in various applications/consumer products.

The total major and trace metal concentrations in unburned vegetation are low (typically 0.11–1.7 wt%) with a mean of 0.56 ± 0.67 wt% and a median of 0.21 wt%. Plants require 17 essential elements for growth: C, H, O, N, P, K, S, Ca, Mg, B, Cl, Cu, Fe, Mn, Mo, Ni, and Zn (Mahler, 2004). Nonetheless, 82 of the 92 elements on Earth can be found in plants (Reimann et al., 2001). Metal concentrations in unburned vegetation are within the range reported elsewhere (Reimann

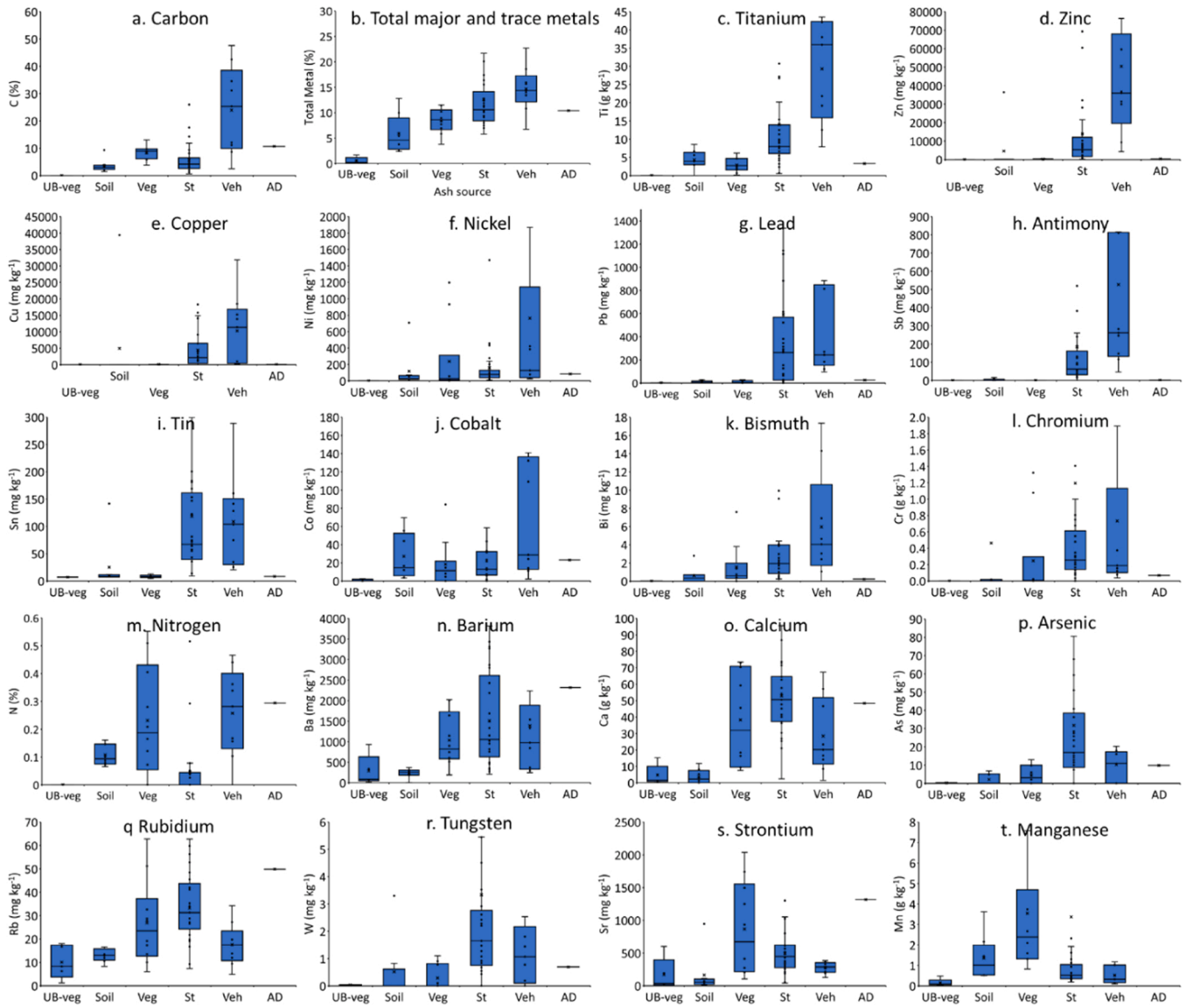

Fig. 1. Elemental concentrations as a function of ash source. UB-veg: unburned vegetation, Veg: vegetation ash, St: structural ash, Veh: vehicle ash, and AD: atmospheric deposition. Elements are ordered by their concentration trend among the different ash types and from highest to lowest concentrations.

et al., 2001). For instance, Ti concentration in unburned vegetation ranges from 11 to 47 mg kg^{-1}, within the reported range of 1–578 mg kg^{-1} (mean: 33.4 mg kg^{-1}) (Reimann et al., 2001). Compared to the unburned vegetation, the total mean major and trace metal content is approximately 15 times higher in the vegetation ashes. Thus, the combustion of vegetation and structural materials at the WUI leaves behind ashes rich in major and trace metals, which account for up to 47 wt% of the ash mass, with a mean of 11.2 ± 6.6 wt% and median of 10.3 wt% major and trace metal concentrations (Fig. 1b).

For each element, the total concentrations in unburned vegetation and vegetation ashes display a wide variability (Figs. S5a **and b**). These variations may be explained by the accumulative capacity of different vegetation types, taking up distinct levels of elements from the soil and surrounding environment (Brito et al., 2017; Peralta-Videa et al., 2009). Fe, Mn, Ti, Ba, Sr, Zn, Ni, and Cu are present in relatively high concentrations in vegetation ash in good agreement with their occurrence in high concentrations in the unburned vegetation, revealing the capacity of these elements to accumulate in plant tissue. This is also consistent with the higher concentration of Ni in vegetation ashes than in soils reported elsewhere (Brito et al., 2017). It is worth noting that the elemental composition of the atmospheric deposition ash (Fig. S5c) is characteristic of the vegetation ash (Fig. S5b). Elements with high concentrations in vegetation ash displayed high concentrations in the atmospheric deposition ash and vice versa. These findings suggest that this atmospheric-deposition ash might have originated dominantly from vegetation ashes, which are expected to be the dominant type of fire ashes during wildfires.

The surprisingly high carbon content in vehicle ashes can be attributed to the thermal stability of black-carbon additives used in vehicle parts such as tires and automobile interiors such as ventilation flaps, radiators, and airbags (Koreňová et al., 2006). For instance, tires consist of mainly carbon-based material, *e.g.,* 70–80 wt% with black carbon accounting for up to 30 wt% (Pehlken and Müller, 2009). The high carbon concentration in vehicle ash also is consistent with the black and gray color of vehicle ashes, which are indicative of high carbon content. The high nitrogen content in vehicle ashes is consistent with those reported in solid tire waste (Islam et al., 2009) and ashes (Cheng et al., 2021). The vulcanization accelerators and plasticizers, commonly added during the production of tires, contribute considerable amounts of nitrogen (*e.g.,* 0.37–0.76 wt%), which remain mostly (*e.g.,* 60–68 %) in the ash after pyrolysis, mainly as a result of the thermal stability of N-containing compounds during pyrolysis (Cheng et al., 2021). Nitrogen is

added to tires in the form of organic heterocyclic-N such as pyrrolic and pyridinic, which partially transform into a more stable structure (Quaternary nitrogen) during pyrolysis, which remains in the ash (Cheng et al., 2021).

The high concentrations of Ti in vehicle and structural ashes are attributed to TiO_2 pigments, the most widely used pigments in paints in vehicles and structures (Fisher and Egerton, 2000). Additionally, many metals are used in various vehicle parts, including brake pads (*e.g.*, Fe, Mn, Ti, Cu, Ba, Zn, Zr, Cr, Ni, Sb, Sn, W, and Pb) (Amato et al., 2012; Borawski, 2020), tires (*e.g.,* Zn accounts for 1–2% of tire weight) (Councell et al., 2004), batteries (*e.g.*, Pb, Sb), and solder (*e.g.,* Sn, Pb, Bi) (United States Geological Survey, 2021), explaining the high concentrations of all measured metals in vehicle ashes. In structures, Zn is widely used in galvanized steel and white paint pigments (Moezzi et al., 2012). Lead was historically used in pigments in structures and can still occur at trace concentrations in pigments that contain Zn (Moezzi et al., 2012). Copper is widely used in water pipes and electrical wires. Barium- and Ca-carbonates are widely used as paint fillers. Arsenic is used in treated wood (Humphrey, 2002). Manganese concentrations are highest in vegetation ashes, consistent with Mn being an essential element for plants and reported with the highest concentration in forest fire ashes (in a number of cases) (Costa et al., 2014; Parra et al., 1996).

3.3. *Elemental concentrations in ash of distinct combustion completeness*

Elemental concentrations exhibit different trends as a function of ash color (Fig. 2). Carbon and N concentrations decrease in the following order: black > gray > gray/red > white ashes (Fig. 2a, b). Calcium, Sr, Rb, and Ag concentrations increase with increased combustion completeness (Fig. 2c-f). Total metal and metalloid concentrations account for 0.4–44.3 wt% of the ash and decrease with combustion completeness (Fig. 2g). Total metal and metalloid concentrations, as well as the concentrations of Zn, Pb, Sn, and In, decrease with increased combustion completeness (Fig. 2h-k).

These trends highlight the different behaviors of elements during fires. During thermal treatment, biomass undergoes drying and pyrolysis

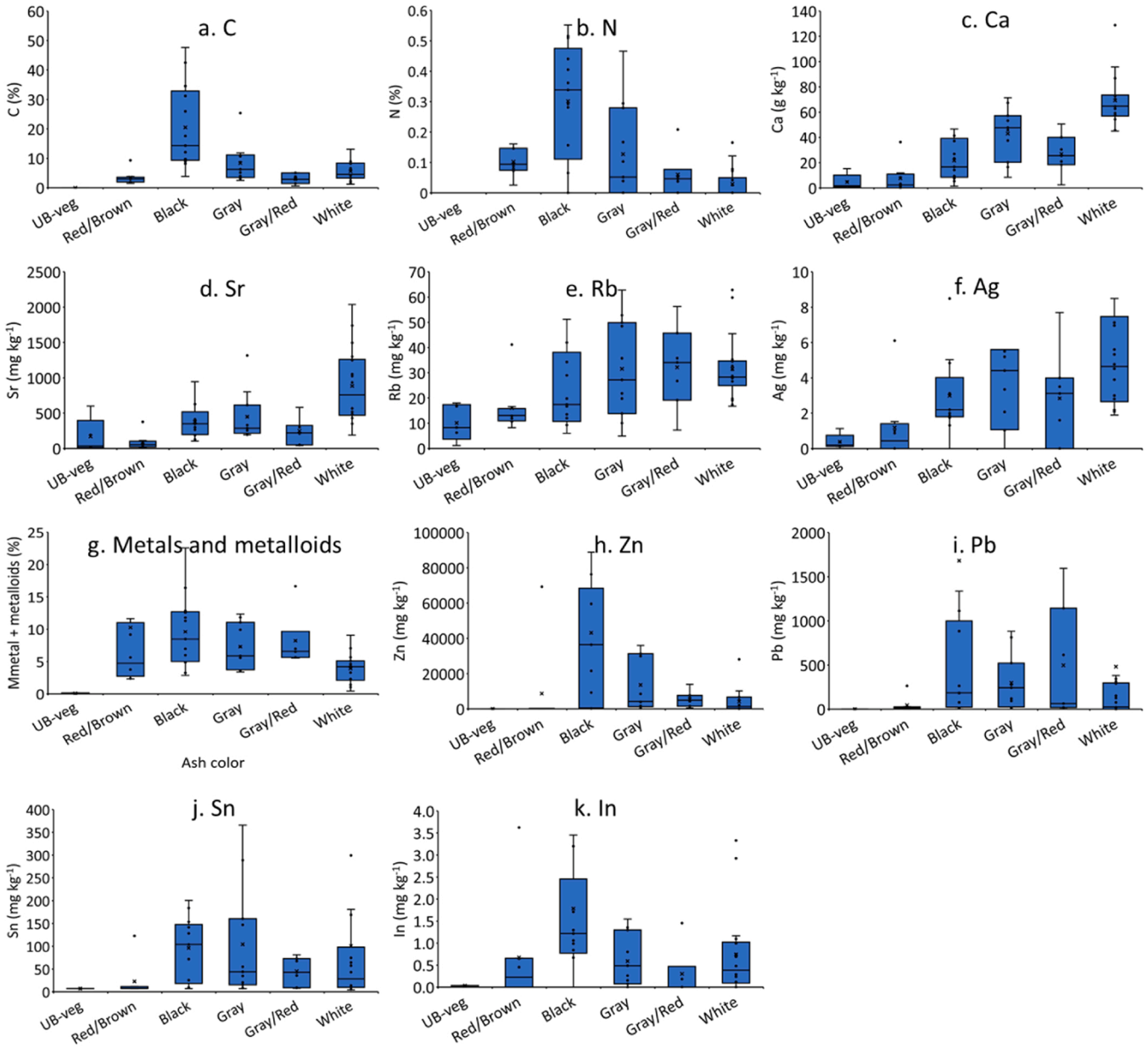

Fig. 2. Elemental concentration as a function of ash color. Elements are ordered by their concentration trend among the different ash types and from highest to lowest concentrations. All other elements did not show any specific trend with ash color.

as a preliminary step. Organic structures disintegrate to give tars, gases, and char, whereas the more volatile inorganics, such as alkali metals and chlorine, volatilize (Badía and Martí, 2003). Thus, the decrease in C concentrations with combustion completeness and the low N concentrations in all ashes can be attributed to the volatilization of C and N at relatively low combustion temperatures. Organic compound volatilization starts at temperatures between 180 and 200 °C, whereas nutrient volatilization starts at temperatures between 200 and 400 °C (Neary et al., 1999). The fate of metals and metalloids atmosphere, metal speciation in fuel, depends on combustion temperature, and metal volatility (Narodoslawsky and Obernberger, 1996; Nzihou and Stanmore, 2013). Some metals (Co and Cu) can be enriched in the residue formed from the burning of biomass, while other metals (Hg) can remobilize as airborne components (fly ash and dust) (Narodoslawsky and Obernberger, 1996; Nzihou and Stanmore, 2013). Fire temperature can exceed the vaporization temperature of various metals (Table S4) resulting in decreases in these metal concentrations in the ashes with increases in fire severity. During combustion, the more volatile metals such as Hg, Pb, Zn, and As tend to vaporize and are released into the atmosphere with smoke. The amount of metal released during a forest fire is limited by their prior accumulation in the fuel and the fire severity (Biswas et al., 2007), which depends on the burn temperature and duration of heating (Neary, Ryan and DeBano, 2005). For example, heating soil for 1 h at 180 °C released < 10 % of the Hg, while heating at 320 °C for 4 h released > 95 % of the Hg (Biswas et al., 2007). Lead volatilizes to a significant extent around 400 °C, As around 600 °C, and Cu and Zn about 800 °C (Han et al., 2006). Other metals (*e.g.*, Mn, Cr, Ni, V, and Co) also vaporize at much higher temperatures (*e.g.,* > 2000 °C, Table S4) (Shao et al., 2008), and thus remain in the fire ash under most WUI fire conditions. The volatilization temperature also depends on the fuel composition and metal speciation (Ljung and Nordin, 1997). For example, in the absence of S and Cl, the solid oxides (CuO and Cu_2O) are stable up to 1100 °C. However, if S and Cl are available in sufficient amounts (> 10 % of S and Cl), the volatilization temperature of CuCl may be as low as 900 °C (Ljung and Nordin, 1997).

3.4. Elemental ratios

The elemental ratios of Ti/Nb, Ni/Fe, and Cr/Fe are higher in several ashes than natural background ratios (Fig. 3), confirming the anthropogenic nature of Ti, Ni, and Cr in the ashes. The Ti/Nb ratio decreases in the following order: vehicle > structure > soil ~ vegetation. The high Ti/Nb ratio in underlying soil samples is likely due to the contamination of some of the soil samples with fire ashes. In particular, NC-13B and NC-13 C have very high Ti/Nb ratios (Fig. S6). The high Ti/Nb ratio in burned vegetation (*e.g.,* 400–5186) might be due to the accumulation of pure Ti in plants (Reimann et al., 2001). The Ni/Fe ratio is highest in vehicle, vegetation, and structural ashes. The Cr/Fe ratio is generally higher in structural and vehicle ashes than in vegetation ashes and unburned vegetations and soils. These trends are consistent with the use of these metals in structures and vehicles, as discussed in Section 3.2. The elemental ratios of Ti/Nb, Cr/Fe, and Ni/Fe did not display any trend with ash color. This is likely due to the high vaporization temperature of these elements (Table S4).

3.5. Anthropogenic Ti concentrations

The concentration of anthropogenic Ti was estimated using mass-balance calculations as performed elsewhere (Loosli et al., 2019) and is at the highest concentrations in vehicle ash followed by structural ashes (Fig. 4). The anthropogenic Ti in soils is likely due to contamination by ashes. The concentration of anthropogenic Ti varied between 4.5 and 41 g kg^{-1} in vehicle ash and between 0 and 77 g kg^{-1} in structural ash. This is consistent with the use of TiO_2 pigments in paint and coatings in structures and vehicles. The global consumption of TiO_2 was estimated at 6.1 million metric tons in 2016 and is projected to reach 8.8 million metric tons by 2025, the majority of which is used as pigments in architectural and industrial paints and coatings (60 %), plastic (28 %), paper (5 %), and other applications (7 %) (Cision, 2020), suggesting a high potential for release of TiO_2 from these sources following fires.

3.6. Transmission electron microscopy analysis

To determine the properties of INMs (*e.g.,* composition, size, morphology) in WUI fire ashes, we performed TEM analyses on a select set of ashes representing different fuel types (vegetation: A31 and A81; structure: A122, A124; A132; vehicle: A13; and structure/vehicle: A131) and ash colors (black: A13, A131, and A132; gray A31 and AD; gray/brown: A124; white: A81 and A122). These samples were also selected as they exhibited high metal concentrations based on ICP-TOF-MS analyzes—A13: Ti, Fe, Pb, Cu, and Zn (Fig. S7a); A31: Fe (Fig. S7b);

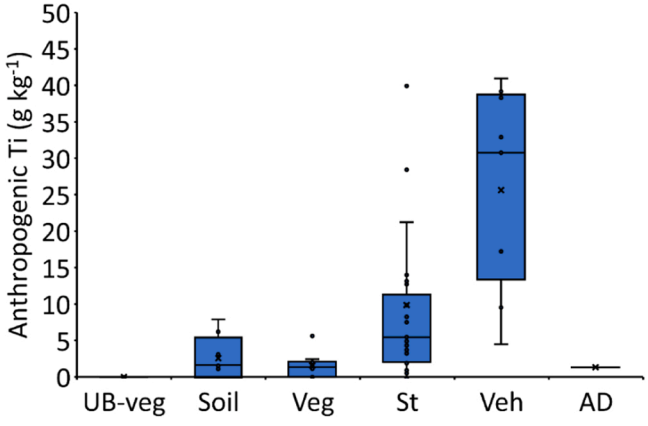

Fig. 4. Concentrations of anthropogenic titanium in ashes as a function of ash source. UB-veg: unburned vegetation, Veg: vegetation ash, St: structural ash, Veh: vehicle ash, and AD: atmospheric deposition.

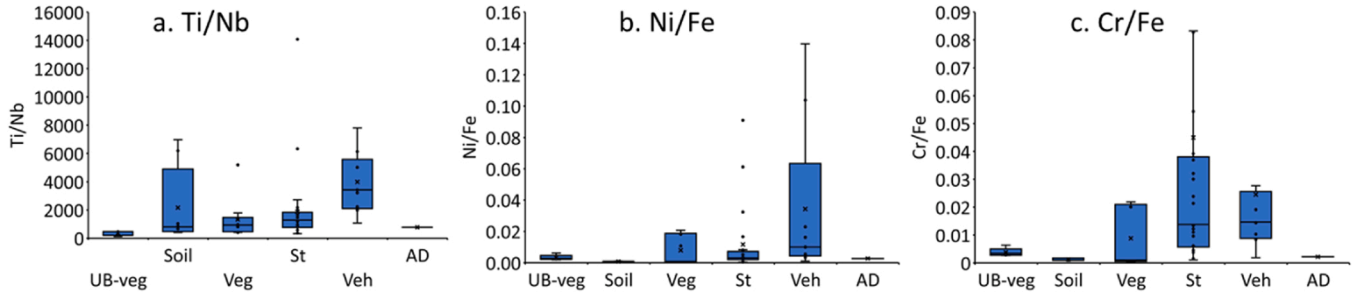

Fig. 3. Elemental ratios as a function of ash source. UB-veg: unburned vegetation, Veg: Vegetation ash, St: structural ash, Veh: vehicle ash, and AD: atmospheric deposition.

A81: Fe, Mn, Sr, Ba, and Ti (Fig. S7c); A122: Ti, Fe, Co, Zn, Pb, and Ba (Fig. S7d); A124: Ti, Fe, Cr, and Zn (Fig. S7e); A131: Zn, Fe, Cu, and Ti (Fig. S7f); A132: Mn, Zn, Fe, and Ti (Fig. S7g); AD: Fe, Mn, Ti, Sr, and Ba (Fig. S7h). The key findings of the TEM analyses are summarized in Table S5 and discussed below.

Different forms of C were observed in the ashes, including turbostratic-like C in A13 (Fig. S8a), turbostratic-like C in association with zinc oxide INMs in A131 (Fig. S8b), and amorphous carbon in A31 (Fig. S8c). In A81, A122, A124, and AD, C was only observed in association with Ca and O, suggesting that it occurs as $CaCO_3$ in these samples (Fig. S9). These forms of C are consistent with ash color, source, and combustion completeness. A13, A131, and AD are black and gray ashes, suggesting that they contain black carbon materials (*e.g.,* turbostratic-like C). On the other hand, A81, A122, A124, and AD are white and gray ashes, indicating higher combustion completeness and transformation of Ca and C to $CaCO_3$. The observation of turbostratic-like C in A13 (vehicle ash) and A131 (structure/vehicle ash) and the association of turbostratic-like C and zinc oxide INMs in A131 are consistent with the high concentration of Zn (8.9%) and C (26 wt%) in A131 and the use of ZnO and black carbon as additives in rubber. Rubber is heavily used in vehicle parts such as tires and automobile interior parts such as ventilation flaps, radiators, and airbags (Koreňová et al., 2006).

Inorganic INMs with various metals (*e.g.,* Ti, Cu, Fe, Zn, Mn, Pb, and Cr) were identified in all of the ash samples with the exception of the vegetation ashes (A31 and A81). The vehicle ash (A13) contains Ca-, Ti-, Cu-, and Zn-bearing INMs, consistent with the elemental composition of this ash sample. Fig. 5 shows an example of INMs observed in ash A13. The aggregate consists of Al-silicate, Ca-carbonate, one Zn-bearing INM, and several Ti-bearing INMs that also contain Cu. The INM size ranges (hereafter listed as the longest dimension for a particle) are as follows: 80–490 nm (n = 18) for Ti-bearing INMs and 120 nm (n = 1) for the Zn-bearing INM. The structural ashes (A122, A124, and A132) and the structure/vehicle ash (A131) contain Ca-, Ti-, Fe-, Cr-, Cu-, Zn-, and Pb-bearing INMs. **In ash A122**, the most frequently detected INMs were Ti-bearing, but other types of INMs, including Ca-, Cr-, Cu-, Fe-, and rare Pb-bearing INMs, are also present. Fig. 6 shows examples of INMs observed in ash A122. The aggregate in Fig. 6a–d consists of an Al-, Si-, Ca-, O-bearing particle, two Ti-bearing INMs, and several Cu-bearing INMs. The aggregate in Fig. 6e–f consists of Al-silicate, Ca-carbonate, several Ti-bearing INMs, and numerous Fe±Cr-bearing INMs. The size ranges of the INMs in A122 are as follows: 40–250 nm (n = 18) for Ti-bearing INMs, 180–270 nm (n = 3) for Cr-bearing INMs, 10–50 nm (n = 13) for Cu-bearing INMs, and 190–270 nm (n = 2) for Fe-bearing INMs. In ash A124, the most frequently observed INMs were Fe- and Ti-bearing INMs; Cu- and Cr-bearing INMs are also present but were observed less frequently. Fig. S10a–d shows an example of INMs observed in ash A124. The aggregate consists of Mg-silicate, Ca-carbonate, several Ti-bearing INMs that contain some Cu, several Fe-bearing INMs, and one Cr-bearing INM. The size ranges of the INMs are as follows: 280–1070 nm (n = 6) for Fe-bearing INMs, 190–440 nm (n = 13) for Ti-bearing INMs, and 90–140 nm (n = 2) for Cr-bearing INMs. In ash A132, the most frequently observed INMs were Ti-, Fe-, and Zn+Cu-bearing INMs. The size ranges of the INMs are as follows: 140–300 nm (n = 7) for Ti-bearing INMs, < 50 nm for Fe-bearing INMs, and 70–450 nm (n = 13) as well as numerous < 50 nm for Zn-bearing INMs. In ash A131, the most frequently observed INMs were Ti- and Zn-bearing INMs. Fig. S10e–h shows an example of INMs from ash A131. The aggregate consists of Al-silicate, Ca-sulfate, five Ti-bearing INMs, and several Zn-bearing INMs. The size ranges of the INMs are as follows:

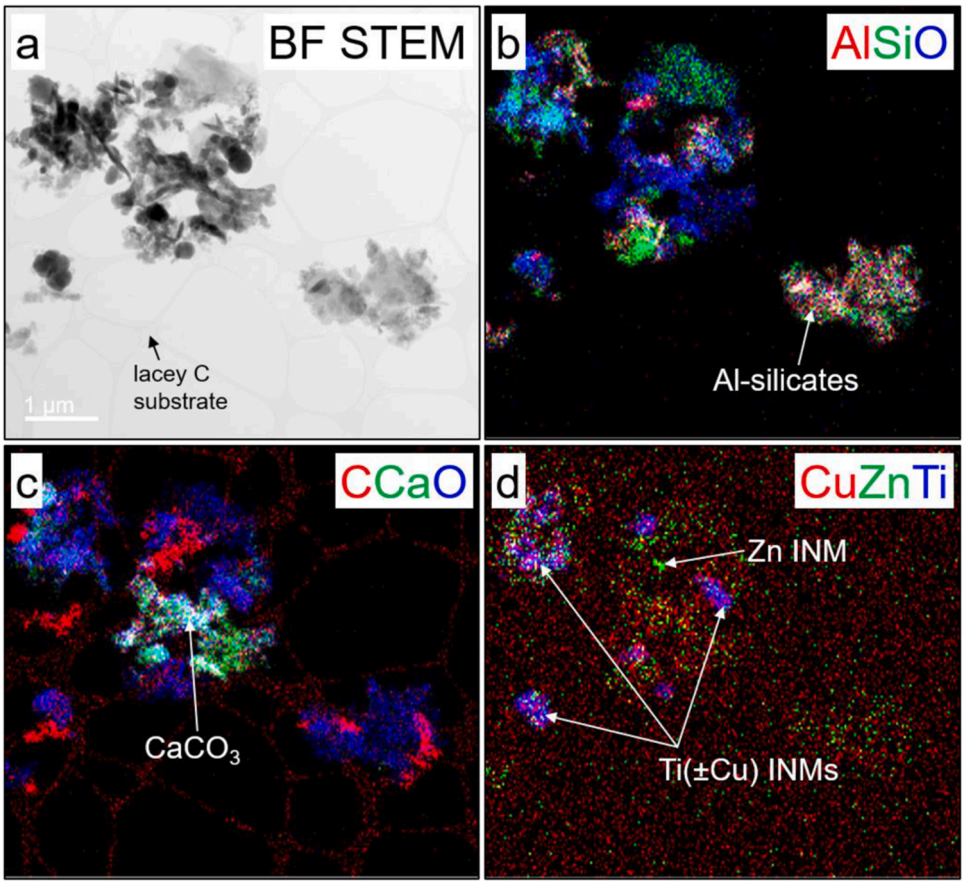

Fig. 5. Representative bright field (BF) TEM image and composite EDS maps showing examples of (b) Al-silicate materials, (c) Ca-carbonate materials, and (d) Ti (± Cu) and Zn INMs identified in vehicle ash A13.

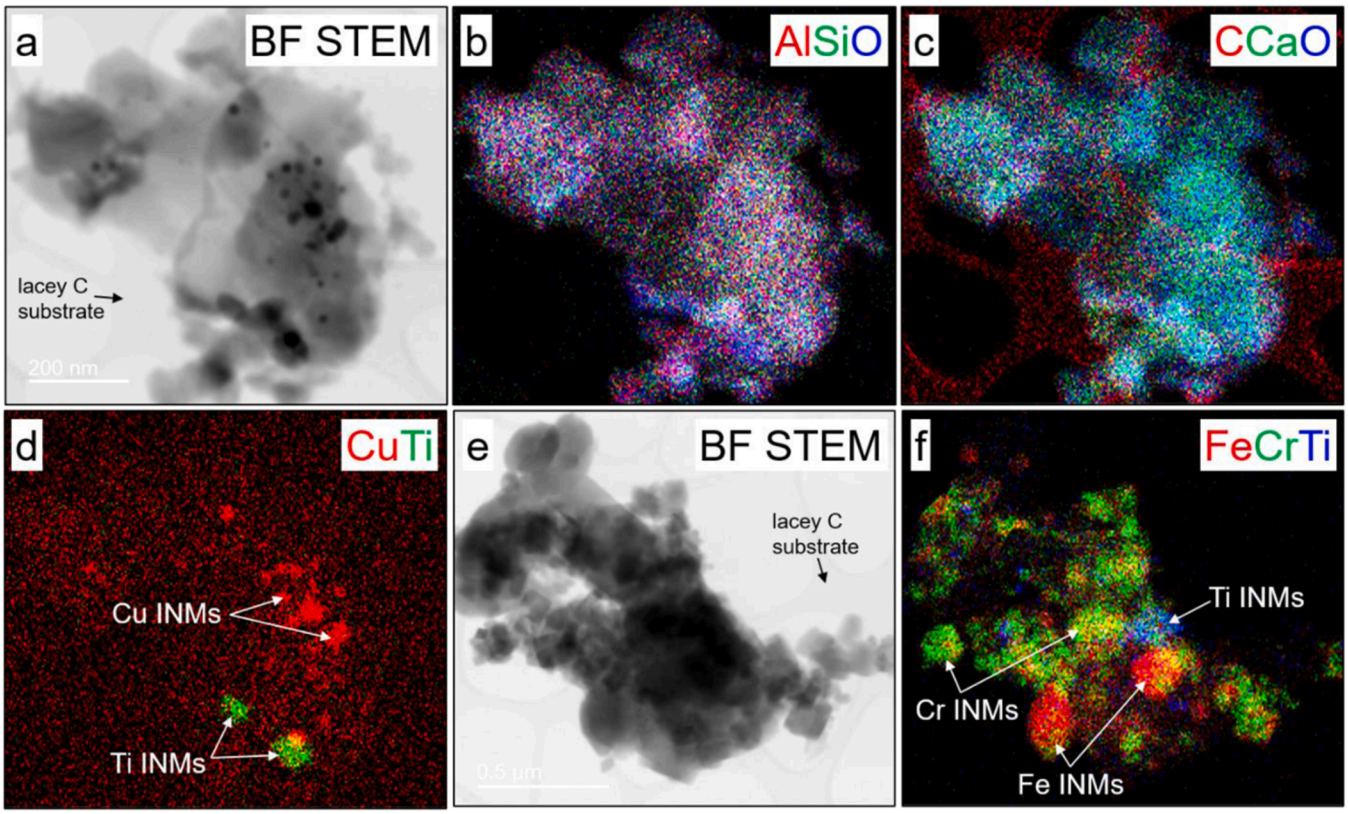

Fig. 6. Representative bright field (BF) TEM images and composite EDS maps showing examples of (b) Al-silicate materials, (c) Ca-carbonate materials, (d) Ti and Cu INMs, and (f) Fe, Ti, and Cr INMs identified in structure ash A122.

50–480 nm (n = 17) for Ti-bearing INMs and 50–250 nm (n = 17) for Zn-bearing INMs. In the atmospheric deposition ash (AD), the most frequently observed particles were $CaCO_3$ particles (Fig. 7b), similar to those observed in the vegetation ashes; however, atmospheric inorganic INMs, such as Fe- and Mn-bearing (Fig. 7c) INMs, were also occasionally identified.

Overall, a total of 73 Ti-bearing and 33 Zn-bearing INMs were identified in the vehicle and structural ashes. The size distribution of Ti-bearing INMs varies between 40 and 500 nm for the longest dimension, with a mean length and width of 210 ± 120 nm and 150 ± 100 nm, respectively (Fig. S11a). Approximately 26% of the Ti-bearing INMs are < 100 nm based on the longest dimensions and 42% are < 100 nm based on the shortest dimensions. These sizes are consistent with those of TiO_2 particles widely used as pigments in paints. Although the size distribution of TiO_2 pigments is predominantly composed of 100–300 nm-sized particles, the particle size range actually extends from the nanoscale (up to 36% of particle number were <100 nm) up to several hundreds of nanometers (Weir et al., 2012). Thus, the majority of TiO_2 pigments contain a fraction of TiO_2 INMs (Weir et al., 2012). It is worth noting that the fraction of nanoscale TiO_2 particles observed in the ashes (26 %) is consistent with those observed in TiO_2 pigments elsewhere (36%) (Weir et al., 2012).

The size distribution of Zn-bearing INMs varied between 50 and 450 nm for the longest dimension, with a mean length and width of 180 ± 120 nm and 120 ± 90 nm, respectively (Fig. S11b). Approximately 39% of the Zn-bearing INMs are < 100 nm based on the longest dimensions and 61% are < 100 nm based on the shortest dimensions. These sizes are typical of those of conventional rubber grade ZnO (*e.g.*,

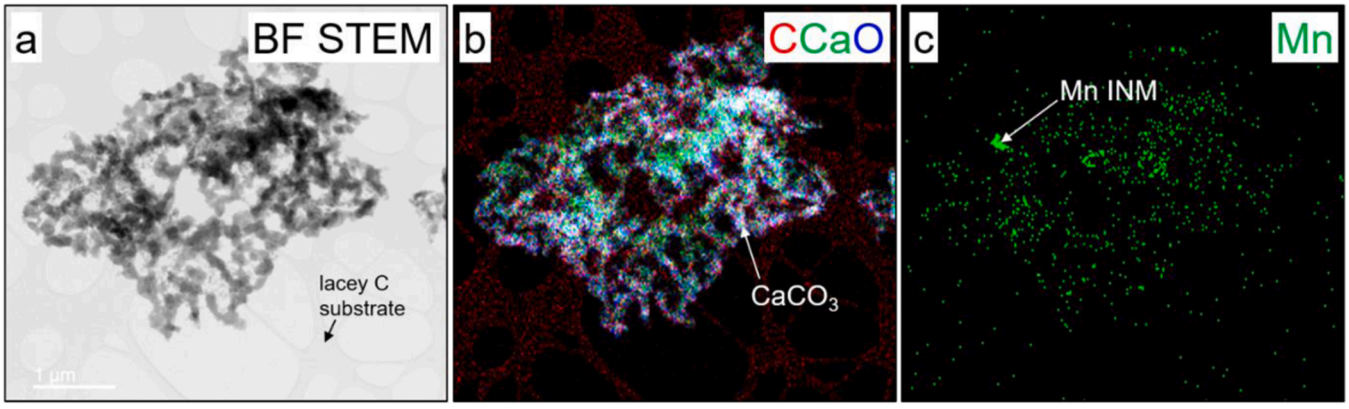

Fig. 7. Representative bright field (BF) TEM image and composite EDS maps showing examples of (b) Ca-carbonate materials and (c) Mn INMs identified in the atmospheric deposition (AD) fire ash sample.

100–400 nm) (George, 2000) and pigment grade ZnO (*e.g.,* < 1000 nm) (Osmond, 2012). The global zinc oxide market size was estimated at over 1.4 million tons in 2021 and is projected to increase at a rate of 4 % in terms of volume between 2022 and 2027 (Mordor Intelligence, 2021). Major applications of zinc oxide include rubber, ceramic, chemical, agriculture, paints and coatings, cosmetics, and pharmaceuticals, as well as other applications (Moezzi et al., 2012). Rubber was the dominant application segment in 2021, accounting for 50–60 % of all ZnO uses, where ZnO is normally added at between 1 and 5 wt% rubber (Moezzi et al., 2012). Global industrial rubber production is estimated at 16 million tons in 2022, about 65 % of which is utilized for the production of tires and automobile interiors such as ventilation flaps, radiators, and airbags (MARKETSANDMARKETS, 2018). A typical tire contains on the order of 100 g of ZnO (Moezzi et al., 2012). Although now largely superseded by TiO_2, ZnO remains an important white inorganic pigment as well.

4. Environmental and human health implications

Results of our analyses indicated that WUI fire ashes contain high concentrations of metals and metalloids, mostly in the form of INMs. The concentrations of Ti, Zn, Cu, Ni, Pb, Sn, Sb, Co, Bi, Cr, Ba, As, Rb, and W are generally higher in structural/vehicle-derived ashes than in vegetation-derived ashes and soils. The concentration of Ca, Sr, Rb, and Ag increase with increased combustion completeness (*e.g.,* black ash < gray ash < white ash), whereas those of C, N, Zn, Pb, and In decrease with combustion completeness. We also demonstrated that fire ashes contain carbonaceous material (turbostratic-like C, amorphous C, and $CaCO_3$) and various metal (Ti, Cu, Fe, Zn, Mn, Pb, and Cr)-bearing INMs with sizes ranging from < 50 nm to a few hundred nms.

The nature and concentration of metal-bearing INMs in fire ashes can be of social and environmental concern, impacting public health and safety, infrastructure, biodiversity, and contributing to land, water, and air pollution. Ash, and its associated contaminants, present potential public health risks to people (*e.g.,* fire recovery workers, residents) and communities through direct and indirect ingestion, inhalation, and skin contact. People are likely to be exposed to the hazardous materials present in the ashes, such as metal and metalloid-bearing INMs, through disturbance and resuspension of the ashes (*e.g.,* from walking, cleaning, wind, and vehicular disturbance), which may be inhaled (Alexakis, 2020). Health effects of ash exposure range from acute symptoms, such as coughing, sneezing, and throat and eye irritation, to chronic disease and increased cancer risk (Reid et al., 2016).

The mobilization of ashes by wind and water poses significant risks to environmental and human health. For instance, one study suggested that ash mobilization by wind to the ocean induces algal growth due to the increased iron supply (Tang et al., 2021). On the other hand, other studies have demonstrated that fire ash extracts induce a significant decrease in the growth of the algae *Raphidocelis subcapitata,* and the common duckweed *Lemna minor* and inhibit the growth of the luminescent the bacteria *Aliivibrio fischeri* (Ré et al., 2020; Silva et al., 2015). Fire ash (from two areas of Cerrado savannah and pasture) has also been shown to be toxic to the zooplankton *Ceriodaphnia dubia* (Brito et al., 2017). Additionally, fire ash runoff, with ash extracts used as a proxy, has been shown to pose hazards to human health due to its cytotoxicity to skin cells, which was attributed to the metals and particles in fire ashes (Ré et al., 2021). Ash from different sources and formed under different fire conditions is likely to possess different toxicities due to the variability in the nature and concentration of metal and metalloid-bearing INMs in WUI ash. For instance, *Eucalyptus* ash was found to be more cytotoxic than pine ash, which was attributed to the different ash metal burden and mobility into the water phase (Ré et al., 2021).

Overall, this study demonstrates the abundance of a variety of metal and metalloid-bearing INMs in WUI fire ashes. At the same time, this study highlights the need for further research into the formation, transformation, reactivity, fate, and effects of INMs during and post fires at the WUI. While experimental work on synthetic nanomaterials can potentially provide insights, additional nanoscience studies of natural environmental samples could help identify unknown transformations of INMs within the fire environment and after release into the environment.

CRediT authorship contribution statement

Mr. Talal Alshehri and Dr. Jingjing Wang performed ash digestion and total metal concentration analysis. Dr. Sheryl A. Singerling performed transmission electron microscopy analysis and the associated data analysis. Dr. Julien Gigault performed carbon and nitrogen analysis. Dr. Jackson P. Webster, Dr. Sandrine J. Matiasek, and Dr. Charles N. Alpers assisted with field sampling campaigns and provided background information on the sampling sites and the collected samples. Dr. Mohammed Baalousha conceived the overall idea of the research, coordinated the collaboration among the research team, supervised Mr. Talal Alshehri and Dr. Jingjing Wang in performing experimental work and data analysis. Mr. Talal Alshehri wrote the first draft of the manuscript. All authors contributed to the manuscript writing and editing.

Declaration of Competing Interest

The authors declare that they have no known competing financial interests or personal relationships that could have appeared to influence the work reported in this paper.

Data Availability

Data will be made available on request.

Acknowledgments

This work was supported by a United States National Science Foundation grants (2101983 and 1828055) and by the Nanoscale Characterization and Fabrication Laboratory and the Virginia Tech National Center for Earth and Environmental Nanotechnology Infrastructure (NanoEarth), a member of the National Nanotechnology Coordinated Infrastructure (NNCI), supported by NSF (ECCS 1542100 and ECCS 2025151). Matthew Uychutin (U.S. Geological Survey, Sacramento, CA) assisted with collection of ash samples. Any use of trade, firm, or product names is for descriptive purposes only and does not imply endorsement by the U.S. Government.

Environmental Implication Statement

This study demonstrated the abundance of a variety of metal and metalloid-bearing incidental nanomaterials (INMs) in wild-urban interface fires (WUI) fire ashes. The accumulation of metals and metalloids in the form of INMs in WUI fire ashes can be of social and environmental concern, impacting public health and safety, infrastructure, and contributing to land, water, and air pollution. Ash, and its associated contaminants, present public health risks to people (*e.g.,* fire recovery workers, residents) and communities through direct and indirect ingestion, inhalation, and absorption. The mobilization of ashes by wind and water to receiving surface waters contaminates drinking water resources.

Appendix A. Supporting information

Supplementary data associated with this article can be found in the online version at doi:10.1016/j.jhazmat.2022.130311.

References

Ahmaruzzaman, M., 2010. A review on the utilization of fly ash. Prog. Energy Combust. Sci. 36 (3), 327–363.

Alexakis, D.E., 2020. Suburban areas in flames: dispersion of potentially toxic elements from burned vegetation and buildings. Estimation of the associated ecological and human health risk. Environ. Res. 183, 109153 https://doi.org/10.1016/j.envres.2020.109153.

Amato, F., Font, O., Moreno, N., Alastuey, A., Querol, X., 2012. Mineralogy and elemental composition of brake pads of common use in Spain. Macla 16, 154–156.

Badía, D., Martí, C., 2003. Plant ash and heat intensity effects on chemical and physical properties of two contrasting soils. Arid Land Res. Manag. 17 (1), 23–41.

Biswas, A., Blum, J.D., Klaue, B., Keeler, G.J., 2007. Release of mercury from Rocky Mountain forest fires. Glob. Biogeochem. Cycles 21 (1).

Bladon, K.D., Emelko, M.B., Silins, U., Stone, M., 2014. Wildfire and the Future of Water Supply. ACS Publications.

Bodí, M.B., Mataix-Solera, J., Doerr, S.H., Cerdà, A., 2011. The wettability of ash from burned vegetation and its relationship to Mediterranean plant species type, burn severity and total organic carbon content. Geoderma 160 (3–4), 599–607.

Bodí, M.B., Martin, D.A., Balfour, V.N., Santín, C., Doerr, S.H., Pereira, P., Cerdà, A., Mataix-Solera, J., 2014. Wildland fire ash: production, composition and eco-hydro-geomorphic effects. Earth-Sci. Rev. 130, 103–127.

Borawski, A., 2020. Conventional and unconventional materials used in the production of brake pads–review. Sci. Eng. Compos. Mater. 27 (1), 374–396.

Brito, D.Q., Passos, C.J.S., Muniz, D.H., Oliveira-Filho, E.C., 2017. Aquatic ecotoxicity of ashes from Brazilian savanna wildfires. Environ. Sci. Pollut. Res. 24 (24), 19671–19682.

Burton, C.A., Hoefen, T.M., Plumlee, G.S., Baumberger, K.L., Backlin, A.R., Gallegos, E., Fisher, R.N., 2016. Trace elements in stormflow, ash, and burned soil following the 2009 station fire in Southern California. PLoS One 11 (5), e0153372.

CALFire, 2022. LNU Lightning Complex (includes Hennessey, Gamble, 15–10, Spanish, Markley, 13–4, 11–16, Walbridge) Incident. ⟨https://www.fire.ca.gov/incidents/2020/8/17/lnu-lightning-complex-includes-hennessey-gamble-15–10-spanish-markley-13–4-11–16-walbridge/⟩.

Campos, I., Abrantes, N., Keizer, J.J., Vale, C., Pereira, P., 2016. Major and trace elements in soils and ashes of eucalypt and pine forest plantations in Portugal following a wildfire. Sci. Total Environ. 572, 1363–1376.

Cheng, Z., Li, M., Li, J., Lin, F., Ma, W., Yan, B., Chen, G., 2021. Transformation of nitrogen, sulfur and chlorine during waste tire pyrolysis. J. Anal. Appl. Pyrolysis 153, 104987. https://doi.org/10.1016/j.jaap.2020.104987.

Cision, 2020. Titanium Dioxide (TiO2) - A Global Market Overview.

Costa, M.R., Calvão, A.R., Aranha, J., 2014. Linking wildfire effects on soil and water chemistry of the Marão River watershed, Portugal, and biomass changes detected from Landsat imagery. Appl. Geochem. 44, 93–102.

Councell, T.B., Duckenfield, K.U., Landa, E.R., Callender, E., 2004. Tire-wear particles as a source of zinc to the environment. Environ. Sci. Technol. 38 (15), 4206–4214.

Dūdaitė, J., Baltrėnaitė, E., Pereira, P., Úbeda, X., 2011. Temperature effects on the ash colour of forest litter. Moksl. ateitis/Sci. Lith. 3 (5), 18–23.

Fisher, J., Egerton, T.A., 2000. Titanium compounds, inorganic. Kirk-Othmer Encycl. Chem. Technol.

George, W., 2000. Handbook of fillers, fourth ed. Elsevier.

Goforth, B.R., Graham, R.C., Hubbert, K.R., Zanner, C.W., Minnich, R.A., 2005. Spatial distribution and properties of ash and thermally altered soils after high-severity forest fire, southern California. Int. J. Wildland Fire 14 (4), 343–354. https://doi.org/10.1071/WF05038.

Griffin, S., Masood, M.I., Nasim, M.J., Sarfraz, M., Ebokaiwe, A.P., Schäfer, K.-H., Keck, C.M., Jacob, C., 2018. Natural nanoparticles: a particular matter inspired by nature. Antioxidants 7 (1), 3.

Han, J., Xu, M., Yao, H., Furuuchi, M., Sakano, T., Kanchanapiya, P., Kanaoka, C., 2006. Partition of Heavy and Alkali Metals during Sewage Sludge Incineration. Energy Fuels 20 (2), 583–590. https://doi.org/10.1021/ef0501602.

Hoover, K., Hanson, L.A., 2021. Wildfire statistics. Congr. Res. Serv. 2.

Humphrey, D.G., 2002. The chemistry of chromated copper arsenate wood preservatives. Rev. Inorg. Chem. 22 (1), 1–40.

Iglesias, T., Cala, V., Gonzalez, J., 1997. Mineralogical and chemical modifications in soils affected by a forest fire in the Mediterranean area. Sci. Total Environ. 204 (1), 89–96. https://doi.org/10.1016/S0048-9697(97)00173-3.

inciweb, 2022. Incident information system. North Complex. ⟨https://inciweb.nwcg.gov/incident/6997/⟩.

Islam, M.R., Haniu, H., Fardoushi, J., 2009. Pyrolysis kinetics behavior of solid tire wastes available in Bangladesh. Waste Manag. 29 (2), 668–677. https://doi.org/10.1016/j.wasman.2008.04.009.

Kaschl, A., Römheld, V., Chen, Y., 2002. The influence of soluble organic matter from municipal solid waste compost on trace metal leaching in calcareous soils. Sci. Total Environ. 291 (1–3), 45–57.

Koreňová, Z., Juma, M., Annus, J., Markoš, J., Jelemenský, L., 2006. Kinetics of pyrolysis and properties of carbon black from a scrap tire. Chem. Pap. 60 (6), 422–426. https://doi.org/10.2478/s11696-006-0077-x.

Lara-Romero, J., Campos-García, J., Dasgupta-Schubert, N., Borjas-García, S., Tiwari, D. K., Paraguay-Delgado, F., Jiménez-Sandoval, S., Alonso-Nuñez, G., Gómez-Romero, M., Lindig-Cisneros, R., Reyes De la Cruz, H., Villegas, J.A., 2017. Biological effects of carbon nanotubes generated in forest wildfire ecosystems rich in resinous trees on native plants. PeerJ 5, e3658. https://doi.org/10.7717/peerj.3658.

Ljung, A., Nordin, A., 1997. Theoretical feasibility for ecological biomass ash recirculation:chemical equilibrium behavior of nutrient elements and heavy metals during combustion. Environ. Sci. Technol. 31 (9), 2499–2503. https://doi.org/10.1021/es960856x.

Loosli, F., Wang, J., Rothenberg, S., Bizimis, M., Winkler, C., Borovinskaya, O., Flamigni, L., Baalousha, M., 2019. Sewage spills are a major source of titanium dioxide engineered (nano)-particle release into the environment. Environ. Sci.: Nano 6 (3), 763–777.

Mahler, R.L., 2004. Nutrients plants require for growth. University of Idaho. College of Agricultural and Life Science CIS, p. 1124.

Markets and Markets, 2018. Industrial Rubber Market by Application. ⟨https://www.marketsandmarkets.com/Market-Reports/industrial-rubber-market-42187401.html⟩.

Miller, J.D., Safford, H., Crimmins, M., Thode, A.E., 2009. Quantitative evidence for increasing forest fire severity in the Sierra Nevada and southern Cascade Mountains, California and Nevada, USA. Ecosystems 12 (1), 16–32.

Moezzi, A., McDonagh, A.M., Cortie, M.B., 2012. Zinc oxide particles: synthesis, properties and applications. Chem. Eng. J. 185–186, 1–22. https://doi.org/10.1016/j.cej.2012.01.076.

E. Moores, J. Moores, M. Hoshovsky, P. Schiffman, B. Schneider, Exploring the Berryessa Region: A geology, nature, and history tour, in memory of Eldridge M. Moores (1938–2018): Backcountry Press., Kneeland, California. (2020).

Mordor Intelligence, 2021. Zinc Oxide Market - Growth, Trends, COVID-19 Impact, and Forecasts (2022 - 2027). ⟨https://www.mordorintelligence.com/industry-reports/zinc-oxide-market⟩.

Narodoslawsky, M., Obernberger, I., 1996. From waste to raw material—the route from biomass to wood ash for cadmium and other heavy metals. J. Hazard. Mater. 50 (2), 157–168. https://doi.org/10.1016/0304-3894(96)01785-2.

Neary, D.G., Klopatek, C.C., DeBano, L.F., Ffolliott, P.F., 1999. Fire effects on belowground sustainability: a review and synthesis. For. Ecol. Manag. 122 (1–2), 51–71.

D.G. Neary, K.C. Ryan, L.F. DeBano, Wildland fire in ecosystems: effects of fire on soils and water. Gen. Tech. Rep. RMRS-GTR-42-vol. 4. Ogden, UT: US Department of Agriculture, Forest Service, Rocky Mountain Research Station. 250 p. 42 (2005).

Nzihou, A., Stanmore, B., 2013. The fate of heavy metals during combustion and gasification of contaminated biomass—a brief review. J. Hazard. Mater. 256–257, 56–66. https://doi.org/10.1016/j.jhazmat.2013.02.050.

Obrist, D., 2007. Atmospheric mercury pollution due to losses of terrestrial carbon pools? Biogeochemistry 85 (2), 119–123.

Oliveira-Filho, E.C., Brito, D.Q., Dias, Z.M.B., Guarieiro, M.S., Carvalho, E.L., Fascineli, M.L., Niva, C.C., Grisolia, C.K., 2018. Effects of ashes from a Brazilian savanna wildfire on water, soil and biota: an ecotoxicological approach. Sci. Total Environ. 618, 101–111. https://doi.org/10.1016/j.scitotenv.2017.11.051.

Osmond, G., 2012. Zinc white: a review of zinc oxide pigment properties and implications for stability in oil-based paintings. AICCM Bull. 33 (1), 20–29. https://doi.org/10.1179/bac.2012.33.1.004.

Parra, J.G., Rivero, V.C., Lopez, T.I., 1996. Forms of Mn in soils affected by a forest fire. Sci. Total Environ. 181 (3), 231–236.

T.R. Peacock, 1992. The preparation of plant material and determination of weight percent ash. US Department of the Interior, Geological Survey.

Pehlken, A., Müller, D.H., 2009. Using information of the separation process of recycling scrap tires for process modelling. Resour. Conserv. Recycl. 54 (2), 140–148. https://doi.org/10.1016/j.resconrec.2009.07.008.

Peralta-Videa, J.R., Lopez, M.L., Narayan, M., Saupe, G., Gardea-Torresdey, J., 2009. The biochemistry of environmental heavy metal uptake by plants: Implications for the food chain. Int. J. Biochem. Cell Biol. 41 (8), 1665–1677. https://doi.org/10.1016/j.biocel.2009.03.005.

Plumlee, G.S., Morman, S.A., Meeker, G., Hoefen, T.M., Hageman, P.L., Wolf, R.E., 2013. The environmental and medical geochemistry of potentially hazardous materials produced by disasters. Treatise Geochem. 9, 257–304.

Radeloff, V.C., Helmers, D.P., Kramer, H.A., Mockrin, M.H., Alexandre, P.M., Bar-Massada, A., Butsic, V., Hawbaker, T.J., Martinuzzi, S., Syphard, A.D., 2018. Rapid growth of the US wildland-urban interface raises wildfire risk. Proc. Natl. Acad. Sci. U.S.A. 115 (13), 3314–3319.

Ragland, K.W., Aerts, D.J., Baker, A.J., 1991. Properties of wood for combustion analysis. Bioresour. Technol. 37 (2), 161–168. https://doi.org/10.1016/0960-8524(91)90205-X.

Ré, A., Campos, I., Saraiva, M.J., Puga, J., Keizer, J.J., Gonçalves, F.J.M., Pereira, J.L., Abrantes, N., 2020. Wildfire effects on two freshwater producers: combining in-situ and laboratory bioassays. Ecotoxicol. Environ. Saf. 194, 110361 https://doi.org/10.1016/j.ecoenv.2020.110361.

Ré, A., Rocha, A.T., Campos, I., Keizer, J.J., Gonçalves, F.J.M., Oliveira, H., Pereira, J.L., Abrantes, N., 2021. Cytotoxic effects of wildfire ashes: In-vitro responses of skin cells. Environ. Pollut. 285, 117279 https://doi.org/10.1016/j.envpol.2021.117279.

Reid, C.E., Brauer, M., Johnston, F.H., Jerrett, M., Balmes, J.R., Elliott, C.T., 2016. Critical review of health impacts of wildfire smoke exposure. Environ. Health Perspect. 124 (9), 1334–1343.

Reimann, C., Koller, F., Frengstad, B., Kashulina, G., Niskavaara, H., Englmaier, P., 2001. Comparison of the element composition in several plant species and their substrate from a 1 500 000-km2 area in Northern Europe. Sci. Total Environ. 278 (1–3), 87–112.

Rutter, A.P., Schauer, J.J., Shafer, M.M., Creswell, J.E., Olson, M.R., Robinson, M., Collins, R.M., Parman, A.M., Katzman, T.L., Mallek, J.L., 2011. Dry deposition of gaseous elemental mercury to plants and soils using mercury stable isotopes in a controlled environment. Atmos. Environ. 45 (4), 848–855.

Scholze, M., Knorr, W., Arnell, N.W., Prentice, I.C., 2006. A climate-change risk analysis for world ecosystems. Proc. Natl. Acad. Sci. U.S.A. 103 (35), 13116–13120.

Shao, J., Yan, R., Chen, H., Yang, H., Lee, D.H., Liang, D.T., 2008. Emission characteristics of heavy metals and organic pollutants from the combustion of

sewage sludge in a fluidized bed combustor. Energy Fuels 22 (4), 2278–2283. https://doi.org/10.1021/ef800002y.
Silva, V., Pereira, J.L., Campos, I., Keizer, J.J., Gonçalves, F., Abrantes, N., 2015. Toxicity assessment of aqueous extracts of ash from forest fires. Catena 135, 401–408. https://doi.org/10.1016/j.catena.2014.06.021.
Sipos, P., Németh, T., Mohai, I., 2005. Distribution and possible immobilization of lead in a forest soil (Luvisol) profile. Environ. Geochem. Health 27 (1), 1–10.
Tang, W., Llort, J., Weis, J., Perron, M.M.G., Basart, S., Li, Z., Sathyendranath, S., Jackson, T., Sanz Rodriguez, E., Proemse, B.C., Bowie, A.R., Schallenberg, C., Strutton, P.G., Matear, R., Cassar, N., 2021. Widespread phytoplankton blooms triggered by 2019–2020 Australian wildfires. Nature 597 (7876), 370–375. https://doi.org/10.1038/s41586-021-03805-8.
U.S. Environmental Protection Agency, 2016. Climate change indicators in the United States, 2016. Fourth edition. EPA 430-R-16–004. ⟨www.epa.gov/climate-indicators⟩.
United States Geological Survey, 2021. Mineral commodity summaries 2021, 200 p., ⟨https://doi.org/10.3133/mcs2021⟩.
Van Der Werf, G.R., Randerson, J.T., Giglio, L., Van Leeuwen, T.T., Chen, Y., Rogers, B. M., Mu, M., Van Marle, M.J., Morton, D.C., Collatz, G.J., 2017. Global fire emissions estimates during 1997–2016. Earth Syst. Sci. Data 9 (2), 697–720.
Wan, X., Li, C., Parikh, S.J., 2021. Chemical composition of soil-associated ash from the southern California Thomas Fire and its potential inhalation risks to farmworkers. J. Environ. Manag. 278, 111570 https://doi.org/10.1016/j.jenvman.2020.111570.
Weir, A., Westerhoff, P., Fabricius, L., Hristovski, K., Von Goetz, N., 2012. Titanium dioxide nanoparticles in food and personal care products. Environ. Sci. Technol. 46 (4), 2242–2250.